AMERICAN SCIENTIFIC PUBLISHERS

Advanced Science Letters
Vol. 3, 1–6, 2010

Nano-Piezoelectricity in $BaTiO_3$: An Atomistic/Continuum Simulation

Xianqiao Wang* and James D. Lee

Department of Mechanical and Aerospace Engineering, George Washington University, Washington, DC 20052 USA

The present work is concerned with the application of Atomistic Field Theory (AFT) in modelling and simulation of polarization and phase transformation in multi-element crystalline materials. Atomistic Field Theory and its corresponding cluster-based numerical implementation are briefly introduced. We have modelled and simulated the dynamic process of polarization and phase transformation in $BaTiO_3$ through coarse-grained finite element simulations, which lends credible support to prove that AFT can capture the atomic-scale material behaviours. Due to the piezoelectric effect of perovskite materials, AFT can offer a more fundamental understanding of energy harvesting from a mechanical system at nanoscale.

1. INTRODUCTION

Piezoelectric materials at nanoscale have attracted increasing attention due to their promising applications in piezoelectric motors,[1] nanoactuators,[2] capacitors,[3] nanogenerators,[4] etc. Nanogenerators offer the potential of harvesting energy from the environment for self-powered nanosystems based on the piezoelectric effect, i.e., a mechanical stress/strain can be converted into polarizations in the material, thereby inducing an electric voltage. Thus, perovskite-type $BaTiO_3$ is a good candidate for nano-piezoelectricity since experiments have demonstrated that $BaTiO_3$ nanowires show a stronger piezoelectric effect than ZnO nanowires under the same amount of mechanical loading.[5]

The experimental advance[6,7] on piezoelectric nanoscale materials has created a concurrently need for a quantitative and predictive understanding of the material behaviour. Various different approaches, including molecular dynamics (MD) simulations and first principle simulations, have been proposed to study the physical phenomena such as size effects,[8] strain effects,[9] etc. However, the massive number of atoms in nano-piezotronics systems renders the first principle or MD simulation powerless or inefficient.

In a series of theoretical papers, an Atomistic Field Theory has been developed by Chen and her co-workers[10–15] for concurrent atomistic/continuum modelling of materials/systems to bridge the gap between microscale and nanoscale. AFT enables us to express an atomic scale local property of a multi-element crystalline system in terms of the distortions of lattice cells and the rearrangement of atoms within the lattice cell, thereby making AFT suitable for a combination of atomistic analysis at fine scale and continuum analysis at coarse scale. In this paper, we model and simulate the dynamic process of polarization and phase transformation in $BaTiO_3$ through coarse-grained finite element simulations.

2. ATOMISTIC FIELD THEORY

To provide the background for the subsequent developments, we briefly review the Atomistic Field Theory constructed by Chen and her coworkers[10–15] and its corresponding numerical algorithm by Lee et al.[15] In contrast with the classical statistical mechanics approaches or the existing formalisms that link unit-cell variables to continuum field variables, AFT views a crystalline material as a continuous collection of lattice cells and a group of discrete atoms situated within each lattice cell as shown in Figure 1. Thus, a more general link, between any phase space function $\mathbf{A}(\mathbf{r},\mathbf{p})$ and its corresponding local density function $\mathbf{a}(\mathbf{x},\mathbf{y}^\alpha,t)$ was developed by Chen[10] as

$$\mathbf{a}(\mathbf{x},\mathbf{y}^\alpha,t)=\sum_{k=1}^{N_l}\sum_{\xi=1}^{N_a}\mathbf{A}(\mathbf{r},\mathbf{p})\delta(\mathbf{R}^k-\mathbf{x})\tilde{\delta}(\Delta\mathbf{r}^{k\xi}-\mathbf{y}^\alpha)$$
$$(\alpha=1,2,3,\ldots,N_a)\quad(1)$$

where the superscript $k\xi$ refers to the ξth atom in the kth unit cell; $\mathbf{R}^k$ is the position of the mass center of the kth unit cell; $\Delta\mathbf{r}^{k\xi}$ is the atomic position of the ξth atom relative to the mass center of the kth unit cell; $\mathbf{x}$ and $\mathbf{y}^\alpha$ are the corresponding physical space counterparts of $\mathbf{R}^k$ and $\Delta\mathbf{r}^{k\alpha}$; N_l is the total number of unit cells in the system; N_a is the number of atoms in a unit cell.

By means of Eq. (1), the local density quantities, such as mass density ρ^α, linear momentum density $\rho^\alpha(\mathbf{v}+\Delta\mathbf{v}^\alpha)$, interatomic force density $\mathbf{f}^\alpha$, external force density $\boldsymbol{\varphi}^\alpha$ are defined

*Author to whom correspondence should be addressed.

Fig. 1. Atomistic view of crystal structure.

in Refs. [14, 15]. The governing equation for linear momentum is, i.e.,

$$\rho^\alpha \ddot{\mathbf{u}}^\alpha(\mathbf{x},t) = -\frac{\gamma^\alpha k_B \nabla T(\mathbf{x},t)}{\Delta V} + \mathbf{f}^\alpha(\mathbf{x},t) + \boldsymbol{\varphi}^\alpha(\mathbf{x},t) \quad (2)$$

where $\dot{\mathbf{u}}^\alpha(\mathbf{x},t) = \mathbf{v} + \Delta\mathbf{v}^\alpha$, $\lambda^\alpha = m^\alpha/m$, and $m = \sum_{\alpha=1}^{N_a} m^\alpha$.

For systems with a given temperature field, the only relevant governing equations are just the balance laws for linear momentum

$$m^\alpha \ddot{\mathbf{u}}^\alpha(\mathbf{x},t) = \mathbf{F}_t^\alpha(\mathbf{x},t) + \mathbf{F}^\alpha(\mathbf{x},t) + \mathbf{F}_{\text{ext}}^\alpha(\mathbf{x},t) \quad (3)$$

where $\mathbf{F}^\alpha(\mathbf{x},t)$ is the interatomic force; $\mathbf{F}_t^\alpha(\mathbf{x},t)$ is the force due to temperature; $\mathbf{F}_{\text{ext}}^\alpha(\mathbf{x},t)$ is the force due to external fields. The existence of superscript α in Eq. (3) implies that the atomic information is naturally built in AFT. Therefore AFT is inherently suitable for multi-element crystalline materials, which is quite different from the classical continuum field theory and many other multiscale theories.

Define $\mathbf{F}^{\xi\eta}[\mathbf{u}^\xi, \mathbf{u}^\eta]$ as the interatomic force acting on an atom whose type and position are indicated by ξ and $\mathbf{u}^\xi$:[15]

$$\mathbf{F}^{\xi\eta}[\mathbf{u}^\xi, \mathbf{u}^\eta] = -\frac{1}{2}\left(\frac{\partial U^{\xi\eta}}{\partial \mathbf{u}^\xi} - \frac{\partial U^{\xi\eta}}{\partial \mathbf{u}^\eta}\right) = \frac{1}{2}(\mathbf{F}^{\xi\eta} - \mathbf{F}^{\eta\xi}) \quad (4)$$

where $U^{\xi\eta}$ is the interatomic potential between the ξ atom and η atom.

For material systems that involve pair atomic interactions, the interatomic force $\mathbf{F}^\alpha(\mathbf{x},t)$ can be expressed as

$$\mathbf{F}^\alpha(\mathbf{x},t) = \int_{\Omega(\mathbf{x}',t)} \frac{1}{\Delta V(\mathbf{x}',t)} \sum_{\beta=1}^{N_a} \mathbf{F}^{\alpha\beta}[\mathbf{u}^\alpha(\mathbf{x},t), \mathbf{u}^\beta(\mathbf{x}',t)] d\Omega(\mathbf{x}',t) \quad (5)$$

where $\Omega(\mathbf{x}',t)$ is the domain associated with the material point $\mathbf{x}'$, and $\Delta V(\mathbf{x}',t)$ is the volume of the unit cell located in $\mathbf{x}'$. It is noticed that, in Eq. (5), full-blown nonlocality and atom-based constitutive relation are automatically rooted in the force calculation. Equations (3), (5) can serve as the governing equation to solve the atomic displacement field, and consequently, atomic-scale properties.

3. NUMERICAL METHODOLOGY

The essences of the novel numerical approach are (1) to reduce the degrees of freedom by the kinematic constraint; (2) to calculate nodal forces with a specified cluster-based summation rule.[16] Some judiciously selected unit cells, called representative unit cells or rep-cells, retain their independent degrees of freedom. Each node in FE mesh is a rep-cell. The nodal displacements together with shape functions are employed to determine a displacement field, in other words, all other unit cells are forced to follow the motion of the nodes—this is what we called "kinematic constraint," which is the practise used in every FE analysis. The continuous displacement filed $\mathbf{u}^\alpha(\mathbf{x})$ is approximated by finite element interpolation from its nodal values $\mathbf{U}_I^\alpha$ as

$$\mathbf{u}^\alpha(\mathbf{x}) = \sum_{I=1}^{N_d} \Phi_I(\mathbf{x}) \mathbf{U}_I^\alpha \quad (6)$$

where $\Phi_I(\mathbf{x})$ is the shape function; N_d is the number of nodes in each element. Following the standard procedure of the Galerkin method, the weak form of Eq. (3) can be written as

$$\int_\Omega \frac{1}{\Delta V(\mathbf{x})} \sum_{\alpha=1}^{N_a} \{m^\alpha \ddot{\mathbf{u}}^\alpha - \mathbf{F}^\alpha - \mathbf{F}_{\text{ext}}^\alpha - \mathbf{F}_t^\alpha\} \cdot \delta\mathbf{u}^\alpha d\Omega = 0 \quad (7)$$

i.e.,

$$\begin{aligned} &\int_{\Omega(\mathbf{x})} \frac{1}{\Delta V(\mathbf{x})} m^\alpha \Phi_J \Phi_I \ddot{\mathbf{U}}_I^\alpha d\Omega(\mathbf{x}) - \int_{\Omega(\mathbf{x})} \frac{1}{\Delta V(\mathbf{x})} \Phi_J \\ &\times \sum_{\beta=1}^{N_a} \int_{\Omega(\mathbf{x}')} \frac{1}{\Delta V(\mathbf{x}')} \mathbf{F}^{\alpha\beta}[\Phi_I \mathbf{U}_I^\alpha, \Phi_K(\mathbf{x}') \mathbf{U}_K^\beta] d\Omega(\mathbf{x}') d\Omega(\mathbf{x}) \\ &- \int_{\Omega(\mathbf{x})} \frac{1}{\Delta V(\mathbf{x})} (\mathbf{F}_t^\alpha + \mathbf{F}_{\text{ext}}^\alpha) \Phi_J d\Omega(\mathbf{x}) = 0 \end{aligned} \quad (8)$$

Then the matrix form of Eq. (8) can be obtained as

$$\tilde{\mathbf{M}}_{IJ} \ddot{\mathbf{U}}_I^\alpha = \tilde{\mathbf{F}}_J^\alpha + \tilde{\mathbf{F}}_{tJ}^\alpha + \tilde{\mathbf{F}}_{\text{extJ}}^\alpha \quad (9)$$

where

$$\tilde{\mathbf{M}}_{IJ} = \int_{\Omega(\mathbf{x})} \frac{1}{\Delta V(\mathbf{x})} m^\alpha \Phi_J \Phi_I d\Omega(\mathbf{x}) \quad (10)$$

$$\begin{aligned} \tilde{\mathbf{F}}_J^\alpha = &\int_{\Omega(\mathbf{x})} \frac{1}{\Delta V(\mathbf{x})} \Phi_J \sum_{\beta=1}^{N_a} \int_{\Omega(\mathbf{x}')} \frac{1}{\Delta V(\mathbf{x}')} \\ &\times \mathbf{F}^{\alpha\beta}[\Phi_I \mathbf{U}_I^\alpha, \Phi_K(\mathbf{x}') \mathbf{U}_K^\beta] d\Omega(\mathbf{x}') d\Omega(\mathbf{x}) \end{aligned} \quad (11)$$

$$\tilde{\mathbf{F}}_{tJ}^\alpha = \int_{\Omega(\mathbf{x})} \frac{1}{\Delta V(\mathbf{x})} \mathbf{F}_t^\alpha \Phi_J d\Omega(\mathbf{x}) \quad (12)$$

$$\tilde{\mathbf{F}}_{\text{extJ}}^\alpha = \int_{\Omega(\mathbf{x})} \frac{1}{\Delta V(\mathbf{x})} \mathbf{F}_{\text{ext}}^\alpha \Phi_J d\Omega(\mathbf{x}) \quad (13)$$

All integrals in Eqs. (10)–(13) are normally carried out by numerical quadrature. In Figure 2, it is seen that around each node (an open circle), say the kth node, there is a cluster (a shaded area), named ψ_k. From now on, force calculation is no longer performed at all unit cells in the entire system but in all clusters. A representative unit cell (a black solid square) is the one within one of $\psi_{I_p} = \{l: |\mathbf{X}_l - \mathbf{X}_{I_p}| \le R_{I_p}\}$. Notice that there is no overlapping of clusters. $\mathbf{X}_l$ is the position of the lth unit cell and R_{I_p} is the radius of the cluster ψ_{I_p} centred at the I_pth node. We postulate that the cluster summation rule reads:

$$\begin{aligned} \tilde{\mathbf{F}}_J^\alpha = &\int_{\Omega(\mathbf{x})} \frac{1}{\Delta V(\mathbf{x})} \Phi_J(\mathbf{x}) \sum_{\beta=1}^{N_a} \int_{\Omega(\mathbf{x}')} \frac{1}{\Delta V(\mathbf{x}')} \\ &\times \mathbf{F}^{\alpha\beta}[\Phi_I(\mathbf{x}) \mathbf{U}_I^\alpha, \Phi_K(\mathbf{x}') \mathbf{U}_K^\beta] d\Omega(\mathbf{x}') d\Omega(\mathbf{x}) \\ \approx &\sum_{I_p=1}^{N_p} n_{I_p} \sum_{j \in \psi_{I_p}} \sum_{k=1}^{N_l} \sum_{\beta=1}^{N_a} \Phi_J(\mathbf{x}_j) \mathbf{F}^{\alpha\beta}[\Phi_I(\mathbf{x}_j) \mathbf{U}_I^\alpha, \Phi_K(\mathbf{x}_k) \mathbf{U}_K^\beta] \end{aligned} \quad (14)$$

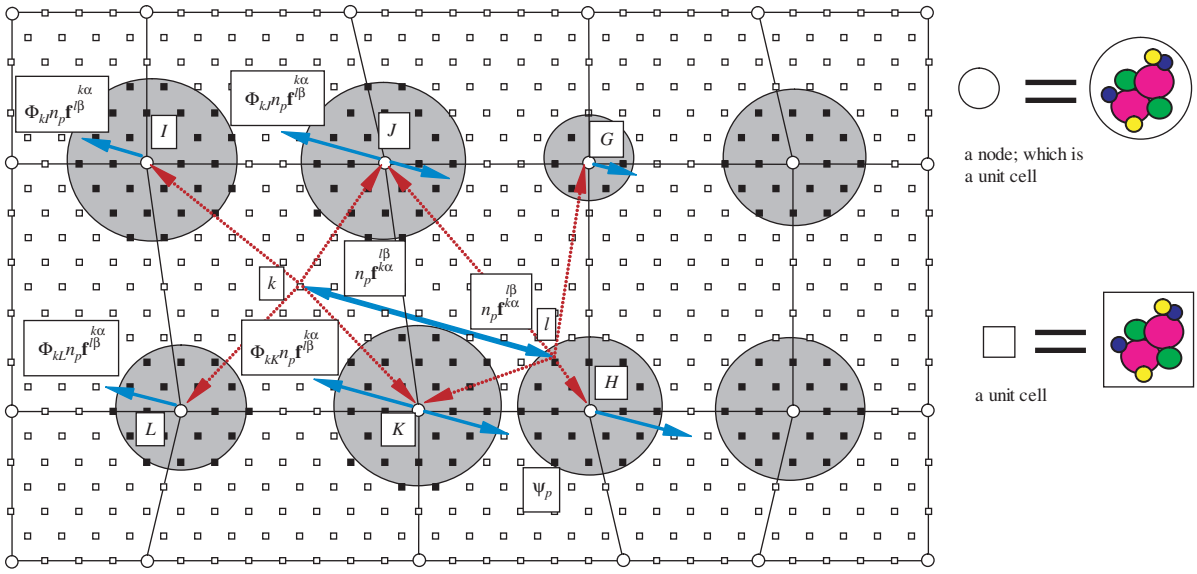

Fig. 2. Schematic picture of AFT model with force distributions.

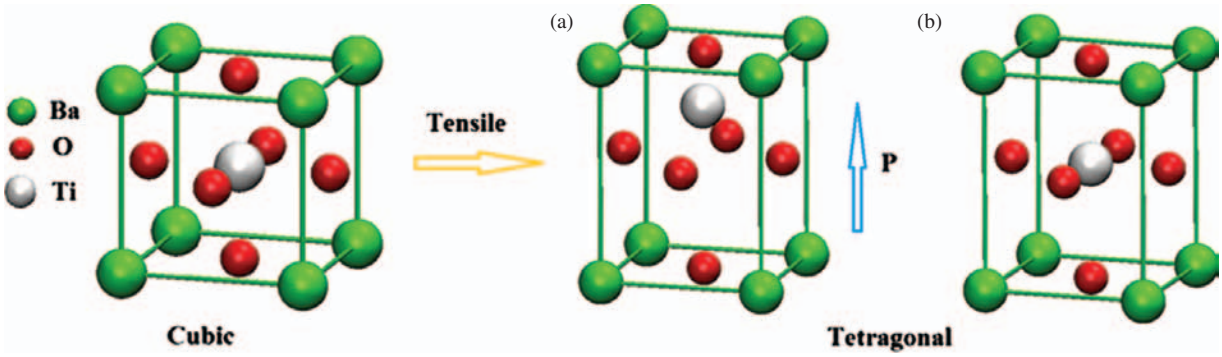

Fig. 3. Polarization in $BaTiO_3$ under tensile or compression loading.

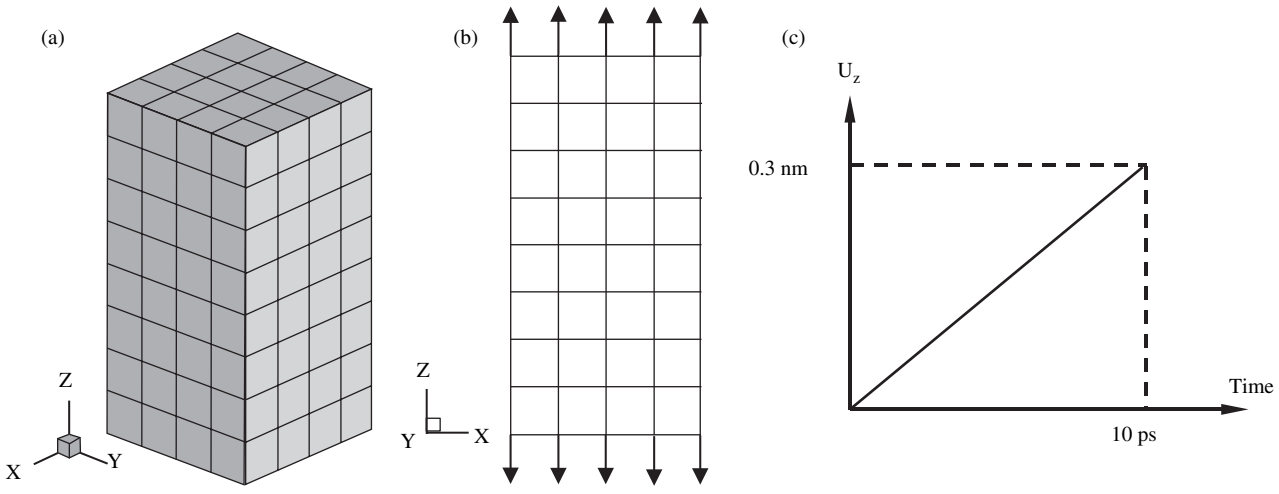

Fig. 4. Computation model: (a) finite element mesh; (b) boundary conditions; (c) loading history.

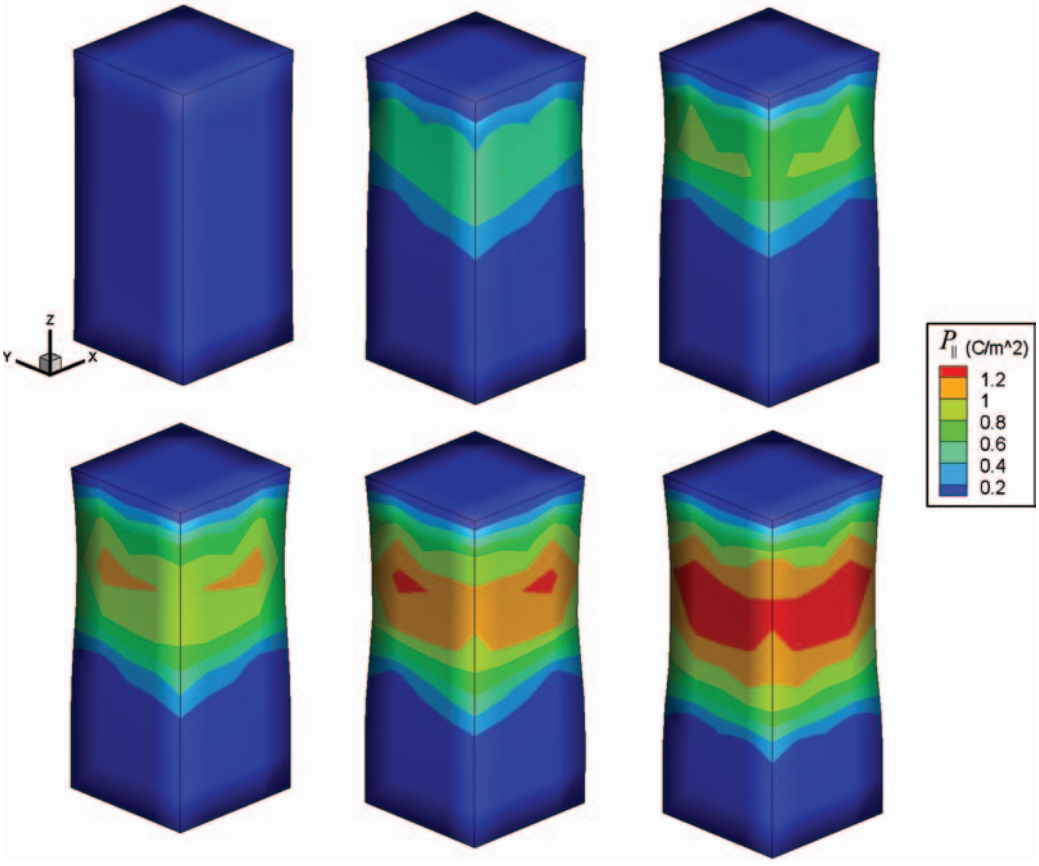

Fig. 5. Polarization $P_{\parallel}$ evolution with time.

where n_{I_p} is the weight of I_pth cluster; N_p is the number of all nodes. When the clusters shrink to the size of the rep-cells, i.e., $\psi_{J_p} = \{J_p\}$, it holds $\Phi_I(\mathbf{x}_{J_P}) = \delta_{IJ_p}$, and the cluster summation rule boils down to a node-based summation rule

$$\mathbf{F}_J^{\alpha} = n_J \sum_{k=1}^{N_l} \sum_{\beta=1}^{N_a} \mathbf{F}^{\alpha\beta}[\mathbf{U}_J^{\alpha}, \Phi_K(\mathbf{x}_k)\mathbf{U}_K^{\beta}] \tag{15}$$

In this case the weighting factor is n_J, which is the number of unit cells represented by Jth node, thus $n_J = \sum_{j=1}^{N_l} \Phi_J(\mathbf{x}_j)$. On the other extreme, $n_J = 1$, implies all pairs of interatomic forces are calculated. In all cases $\sum_{I_p} \sum_{j \in \psi_{I_p}} n_{I_p} = N_l$ holds.

4. POLARIZATION

The piezoelectric material $BaTiO_3$ has a centrosymmetric cubic crystal structure as a reference nonpolar state, and polarization is defined with respect to the nonpolar state (Fig. 3) and is a function of internal atomic displacements. It is noticed in Figure 3 that the unit cell becomes tetragonal structure under the tensile strain. When the interior atoms are allowed to move independently, one may encounter a non-centrosymmetric structure which gives a polarization (Fig. 3(a)). On the other hand, if we follow Cauchy-Born rule[17] strictly, then the tetragonal structure is still centrosymmetric and hence it yields no polarization (Fig. 3(b)). From Eq. (3), which governs the motion of every atom in unit cells, it is seen that the internal atomic displacements have been naturally incorporated in our formulations. In AFT, it is straightforward to show the polarization density $\mathbf{P}(\mathbf{x}, t)$ of a lattice point as

$$\begin{aligned} \mathbf{P}(\mathbf{x}, t) &= \sum_{k=1}^{N_l} \sum_{\alpha=1}^{N_a} q^{k\alpha}(\mathbf{R}^k + \Delta\mathbf{r}^{k\alpha})\delta(\mathbf{R}^k - \mathbf{x}) \\ &= \sum_{k=1}^{N_l} \sum_{\alpha=1}^{N_a} q^{k\alpha} \Delta\mathbf{r}^{k\alpha} \delta(\mathbf{R}^k - \mathbf{x}) \end{aligned} \tag{16}$$

In this numerical simulation, a nanosize $BaTiO_3$ specimen (1.6 nm × 1.6 nm × 3.2 nm, 6885 atoms) subject to a tensile loading is modelled with 128 finite elements and 225 nodes. Thus the number of the degrees of freedom involved in AFT is about 3.2% of that in MD. The displacement controlled boundary conditions with a constant velocity 30 m/s are applied on both ends of the specimen and the total loading time is 10 ps (Fig. 4).

As shown in Figure 3, when the specimen is subject to a tensile loading in the z-direction, an expected polarization will appear in the z-direction. Figure 5 shows the contour plots of polarization $P_{\parallel}$ along the z-direction. It is observed that the polarization $P_{\parallel}$ become more pronounced as time goes. It is noticed that the maximum value of $P_{\parallel}$ is about 1.2 C/m^2. Here we define $P_{\perp} \equiv \sqrt{\mathbf{P}_x \cdot \mathbf{P}_x + \mathbf{P}_y \cdot \mathbf{P}_y}$ to characterize the magnitude of the polarization on the x–y plane. Figure 6 shows the contour plots of polarization $P_{\perp}$ as time goes on. It is observed that the polarizations, $P_{\parallel}$ and $P_{\perp}$, easily appear at the edges since the symmetry of

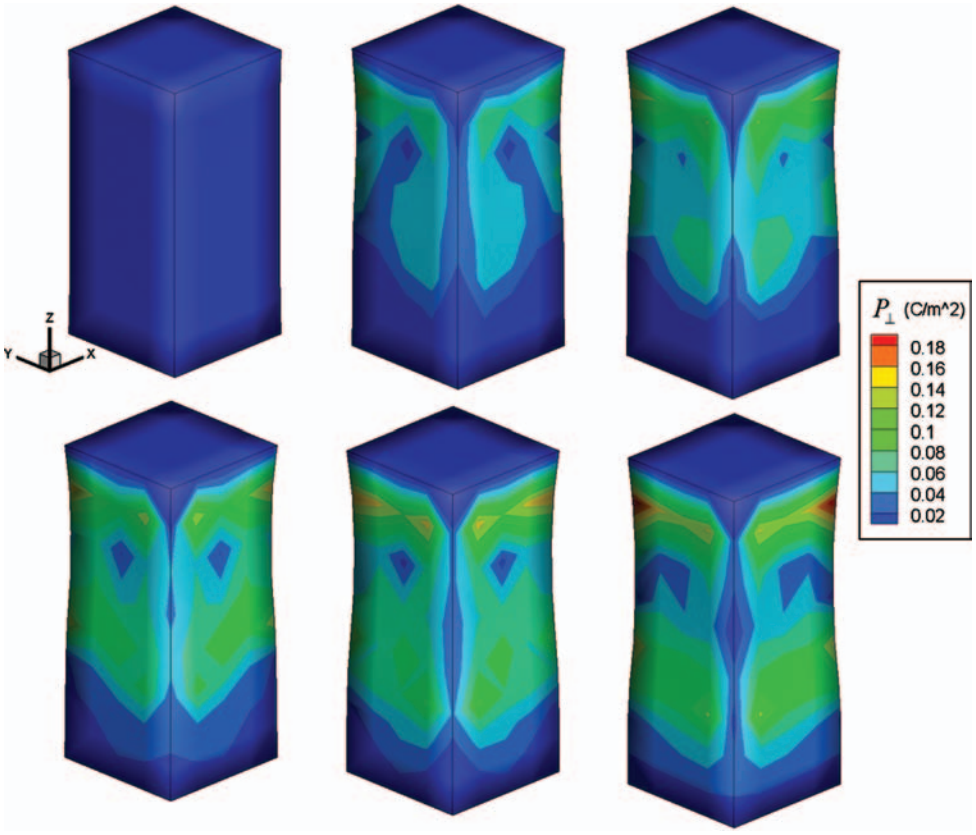

Fig. 6. Polarization $P_\perp$ evolution with time.

lattice cell is more vulnerable to break under the tensile loading. Also, polarizations accompany the phenomenon of necking. Compared with $P_\parallel$, which is the primary effect under tension, the secondary effect $P_\perp$ is much smaller as expected. Figure 7 shows the dynamic process of phase transformation in one unit cell: from Figure 7(a), the top view of the specimen, the structure appears to be symmetric—that is why $P_\perp$ is insignificant; from Figure 7(b), the side view of the specimen, one notices that the Ti atom moves upward and deviates from its central position—that is why $P_\parallel$ is much pronounced.

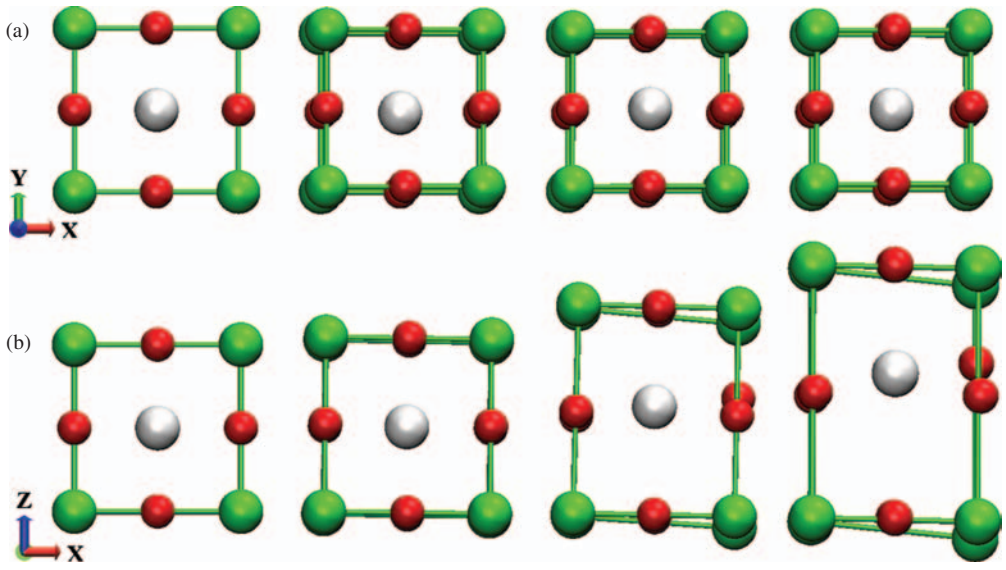

Fig. 7. Dynamic process of phase transformation in $BaTiO_3$: (a) top view; (b) side view.

5. CONCLUSIONS

This paper presented the simulation results of nano-piezoelectricity in $BaTiO_3$. By virtue of Atomistic Field Theory, we have revealed the deformation mechanisms as well as the local phase transformation of nano-crystalline $BaTiO_3$ under tensile loading. Results have demonstrated that AFT offers the possibility to study piezoelectricity, energy harvesting and electrodynamics at the nano scale from an atomistic/continuum perspective.

References and Notes

1. O. Auciello, J. F. Scott, and R. Ramesh, *Phys. Today* 51, 22 **(1998)**.
2. J. Gaspar, V. Chu, and J. P. Conde, *J. Appl. Phys.* 93, 10018 **(2003)**.
3. D. K. Lee, D. W. Kim, I.-S. Cho, S. Lee, J. Noh, and K. S. Hong, *J. Nanosci. Nanotechnol.* 10, 1361 **(2010)**.
4. Z. L. Wang and J. H. Song, *Science* 312, 242 **(2006)**.
5. A. Wang, J. Hu, A. P. Suryavanshi, K. Yum, and M. F. Yu, *Nano Lett.* 7, 2966 **(2007)**.
6. J. He, J. C. Jiang, J. Liu, G. Collins, C. L. Chen, B. Lin, V. Giurgiutiu, R. Y. Guo, A. Bhalla, and E. I. Meletis, *J. Nanosci. Nanotechnol.* 10, 6245 **(2010)**.
7. S.-M. Moon, C. Lee, J.-W. Han, and N.-H. Cho, *J. Nanosci. Nanotechnol.* 9, 1518 **(2009)**.
8. Y. Zhang, J. Hong, B. Liu, and D. Fang, *Nanotechnology* 20, 405703 **(2009)**.
9. Y. Zhang, J. Hong, B. Liu, and D. Fang, *Nanotechnology* 21, 015701 **(2010)**.
10. Y. Chen and J. D. Lee, *Philos. Mag.* 85, 4095 **(2005)**.
11. Y. Chen, *J. Chem. Phys.* 124, 054113 **(2006)**.
12. L. Xiong, Y. Chen, and J. D. Lee, *J. Nanosci. and Nanotechnol.* 8, 1 **(2008)**.
13. Y. Chen, *J. Chem. Phys.* 130, 134706 **(2009)**.
14. J. D. Lee, X. Wang, and Y. Chen, *J. Eng. Mech-ASCE* 135, 192 **(2009)**.
15. J. D. Lee, X. Wang, and Y. Chen, *Theor. Appl. Fract. Mech.* 51, 33 **(2009)**.
16. B. Eidel and A. Stukowski, *J. Mech. Phys. Solids.* 57, 87 **(2009)**.
17. J. L. Ericksen, *Math. Mech. Solids.* 13, 199 **(2008)**.

Received: 26 May 2010. Accepted: 2 June 2010.